Chemical Compounds of Water-Soluble Impurities in Dome Fuji Ice Core

Yoshinori Iizuka, Hiroshi Ohno[#], Toshimitsu Sakurai, Shinichiro Horikawa, Takeo Hondoh

Institute of Low Temperature Science, Hokkaido University, Sapporo, Japan,
iizuka@lowtem.hokudai.ac.jp
[#]present address: Center for Hydrate Research, Colorado School of Mines, Golden, Colorado, USA

Abstract: The amounts of water-soluble impurities in ice cores have been widely discussed in past research on prehistoric climates; in those studies, the analysis of the soluble-aerosol signals of several ion concentrations took place after the ice cores were melted. However, the chemical compounds of the impurities being studied were unclear, due to the ionization of the impurities being caused by the melting of the ice cores. In this paper, the chemical compounds of water-soluble impurities in Dome Fuji ice core are discussed and analyzed using micro-Raman spectroscopy and ion chromatography. Raman spectroscopy helped identify micro-inclusions within ice grains as water-soluble impurities made up primarily of sodium sulfate formed in warm periods and calcium sulfate in cold periods. The major chemical compounds of the water-soluble impurities (sodium sulfate and calcium sulfate) were deduced by examining ion concentrations and the stability of chemical compounds. The amounts of impurities reflect the differences in climatic time periods, as the environment was acidic during warm times and reductive during cold.

Key words: salt inclusion, water-soluble impurities, Dome Fuji ice core, Raman spectroscopy

1. Introduction

Ice cores drilled from the inland regions of polar ice sheets can be used to reconstruct past environments and climates over the past several hundred thousand years, a period that includes several glacial cycles. Long-term paleoclimate studies have been carried out on ice cores from Byrd [1], Vostok [2], Dome Fuji [3], EPICA DML [4], and EPICA Dome C [5] in Antarctica.

A useful technique for reconstructing past environments and climates in these ice cores is the determination of dissolved ion species [6] by chromatography [7] or continuous flow analysis [8]. For example, sodium ions may be considered as a proxy for the amount of sea ice that formed around the polar ice sheet, while calcium ions can be used as a proxy for the amount of terrestrial material in Antarctica [9]. The potential of this technique for reconstructing past environments is not limited to the above examples; it is also possible to reconstruct aerosol compositions. However, the chemical makeup of compounds with aerosol compositions is unclear due to the ionization of water-soluble impurities caused by the melting of the ice core.

The deduction of the chemical compounds of water-soluble impurities is conducted by analyzing ion concentrations [10, 11]. As part of the deduction, post-depositional processes [12, 13, 14] and chemical reactions [15] are considered to affect the amounts and forms of ion species. Table 1 shows the primary chemical reactions involving the Cl^-, NO_3^-, SO_4^{2-}, Na^+, Mg^{2+}, and Ca^{2+} species in Antarctica. To summarize the findings obtained so far in previous research, Na_2SO_4 was the most common salt during the Holocene due to reaction (1), which occurs in the atmosphere [16] and firn [17]. During the last Glscial Maximum (LGM) however, $CaSO_4$ was more common due to reaction (4). This reaction also occurs in the atmosphere [16] and firn [18]. $NaNO_3$ molecules were created in the atmosphere by reaction (2) [19]. The post-depositional process of HNO_3, was important in Antarctica during the Holocene [20]. During the LGM, $Ca(NO_3)_2$ was produced in the atmosphere and firn by reaction (5) whenever the Ca2+ concentration exceeded 20 ppb [18]. Finally, the post-depositional process of HCl by reactions (1) and (2) in inland areas was important during the Holocene [18, 20]. During the LGM, reaction (4) prevented reaction (1) and preserved sea salts (NaCl, $MgCl_2$) instead [20].

In this paper, an analysis of chemical compounds of water-soluble impurities in Dome Fuji ice using micro-Raman spectroscopy (RS) and ion chromatography (IC) is discussed with a review of some of the authors' recent papers [17, 21, 22, 23]. RS enables the identification of the chemical compounds of impurities—air bubbles, clathrate hydrates, insoluble dust, soluble salts, and so on—in ice grains if the impurity has materials with Raman activity. However, when applying the results of micro-Raman analysis to reconstructing past environments, it is important to determine the correct relationship between ion concentrations and the quantities of identified salt compounds. The method used in this paper relates ion concentrations analyzed by IC to the chemical compounds of salt inclusions as observed by RS.

2. Analytical methods

The ice core used in this study was from the Dome Fuji (DF) station, which is located at the summit of East

Dronning Maud Land Plateau (3810 m above sea level), East Antarctica. The ice core was 2500 m long and is a record of the past 340 kyrBP [24]. At the DF site, the present-day temperature averages –58 ˚C and the accumulation rate averages 32 mm of water equivalent per year. The Dome-F Deep Coring Group [25] has more detailed information on the geophysical setting of the station.

Table 1: The primary chemical reactions concerning Cl^-, NO_3^-, SO_4^{2-}, CO_3^{2-}, Na^+, Mg^{2+}, and Ca^{2+} species in Antarctica [23]. The one-way and two-way arrows indicate chemical reactions and equilibriums respectively. The priority sequence indicates that $CaSO_4$ is formed first, followed by other sulfate salts, nitrate, chloride, and carbonate in that order. The reasons for these priorities are discussed in the text.

NO.	Reaction situation	Reaction formula	Reaction priority
[1]	Chloride salts (NaCl, $MgCl_2$) reaction to sulfate	$2NaCl + H_2SO_4 \Leftrightarrow 2Na_2SO_4 + HCl$ $MgCl_2 + H_2SO_4 \Leftrightarrow MgSO_4 + 2HCl$	2 (when less $[Ca^{2+}]$ than $[H_2SO_4]$)
[2]	Chloride salts (NaCl, $MgCl_2$) reaction to nitrate	$NaCl + HNO_3 \Leftrightarrow NaNO_3 + HCl$ $MgCl_2 + 2HNO_3 \Leftrightarrow Mg(NO_3)_2 + 2HCl$	4 (when absence of carbonate and H_2SO_4)
[3]	Nitrate salts from sea salts [2] reaction to sulfate	$2NaNO_3 + H_2SO_4 \Leftrightarrow Na_2SO_4 + 2HNO_3$ $Mg(NO_3)_2 + H_2SO_4 \Leftrightarrow MgSO_4 + 2HNO_3$	2 (when less $[Ca^{2+}]$ than $[H_2SO_4]$)
[4]	Carbonate salts ($CaCO_3$, $MgCO_3$) reaction to sulfate	$CaCO_3 + H_2SO_4 \rightarrow CaSO_4 + H_2O + CO_2$ $MgCO_3 + H_2SO_4 \rightarrow MgSO_4 + H_2O + CO_2$	1 2 (when less $[Ca^{2+}]$ than $[H_2SO_4]$)
[5]	Carbonate salts ($CaCO_3$, $MgCO_3$) reaction to nitrate	$CaCO_3 + 2HNO_3 \rightarrow Ca(NO_3)_2 + 2H_2O + CO_2$ $MgCO_3 + 2HNO_3 \rightarrow Mg(NO_3)_2 + 2H_2O + CO_2$	3 (when absence of H_2SO_4)
[6]	Nitrate salts from carbonate salts [5] reaction to sulfate	$Ca(NO_3)_2 + H_2SO_4 \Leftrightarrow CaSO_4 + 2HNO_3$ $Mg(NO_3)_2 + H_2SO_4 \Leftrightarrow MgSO_4 + 2HNO_3$	1 2 (when less $[Ca^{2+}]$ than $[H_2SO_4]$)

2.1. Micro-Raman spectroscopy (RS)

After arriving in Japan, the ice core was stored in a cold room at –50 ˚C and prepared in a cold room at –20 ˚C. The ice core was cut with a band saw into 80 × 40 × 5 mm^3 sections from depths of 185, 362, 576, 1122, 1351, 1746, 1919, 2280, and 2413 m; the upper and lower surfaces of each section were then planed with a microtome [21, 22]. The ages of these ice sections are 5.6, 12.0, 24.7, 69.1, 87.8, 130.1, 157.4, 244.1, and 298.8 kyrBP, respectively. Observations of micro-inclusions in the sections were done in a cold room at –15 ˚C. To obtain the average number concentration of micro-inclusions (N) over a section, 100 regions of dimensions 0.18 × 0.40 × 5 mm^3 were randomly picked and the number of inclusions was counted in each region. The standard error of N was about ±12%. To obtain the mean equivalent-sphere diameter of micro-inclusions Di for a given section, the minimum and maximum diameters of 100 inclusions were averaged from the inside and outside of their outlines.

Ice specimens of size 10 × 10 × 3 mm^3 were cut from the original 80 × 40 × 5 mm^3 sections and prepared in a cold chamber on an x–y translation stage of a microscope. The chamber was kept at –30±0.5 ˚C during the measurements by regulating the flow rate of cold N_2 gas. A laser of wavelength 514.5 nm and power 100 mW was focused to a diameter of about 1 Am on the specimen using a long-working distance objective lens with a 6-mm focal length (Mitutoyo, M Plan Apo 100). Back-scattered Raman spectra were obtained using a triple monochromator (Jobin-Yvon, T64000) equipped with a CCD detector. The absolute frequency of the monochromator was calibrated with neon emission lines. The spectral resolution obtained was 1.8 cm^{-1} for a single dispersion case and 0.6 cm^{-1} for a triple dispersion case at 600 nm with an entrance slit of 100 Am [21]. Thirty micro-inclusions per section were measured.

To identify the chemical compositions in the

inclusions, the observed spectra were compared with reference specimens for sulfate salts ($Na_2SO_4 \cdot 10H2O$, $MgSO_4 \cdot 12H_2O$, $CaSO_4 \cdot 2H_2O$, and K_2SO_4), nitrate salts ($NaNO_3$, $Mg(NO_3)_2 \cdot 6H_2O$, $Ca(NO_3)_2 \cdot 4H_2O$, and KNO_3) and acid solutions (H_2SO_4, HNO_3 and CH_3SO_3H). $Na_2SO_4 \cdot 10H_2O$ and $MgSO_4 \cdot 12H_2O$ were obtained by freezing 15 wt.% solutions at –15 ˚C. $CaSO_4 \cdot 2H_2O$, K_2SO_4 and all the nitrate salts are chemicals that are commercially available. For the acids, pieces of the ice core were left in 20 wt.% solutions at –30 ˚C for 2 days, after which the solution were then measured. The reference data is shown in Fig. 1.

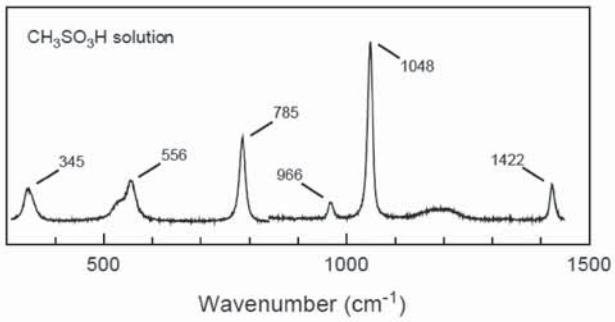

Figure 1a: Raman spectra of the reference specimen for CH_3SO_3H [21].

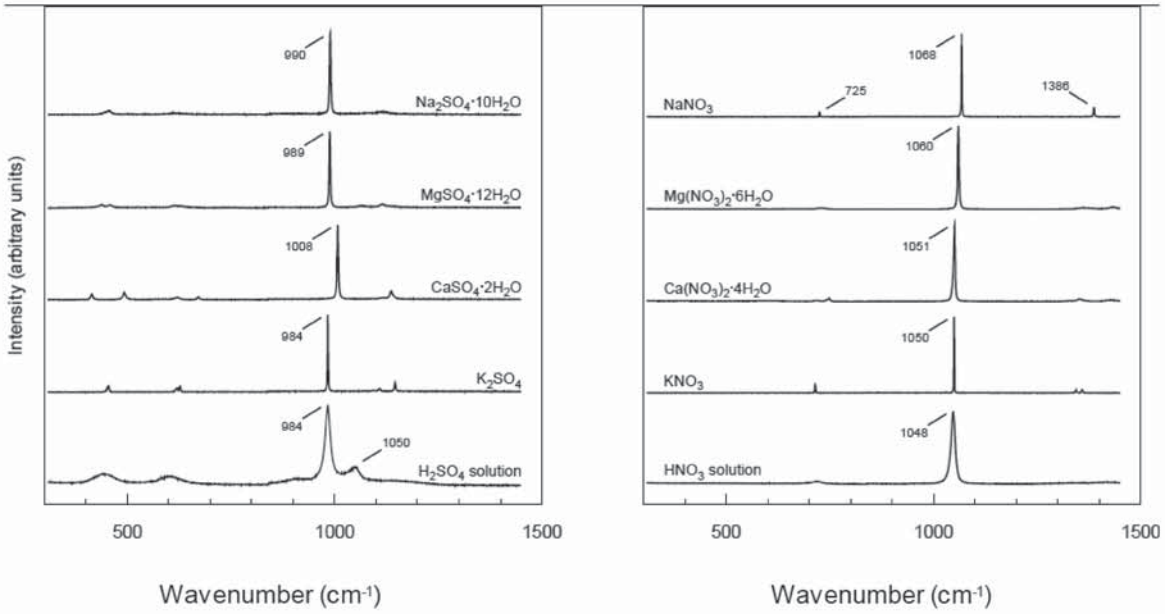

Figure 1b: Raman spectra of the reference specimens for various salts and acids [21].

2.2. Ion chromatography (IC)

Ice sections of 500 mm lengths were selected at three separate depths well away from each other: 119 m (119.291 to 119.770 m), 298 m (298.403 to 298.878 m), and 415 m (415.352 to 415.818 m) [17, 23, 26]. The ages of these ice sections are 3.0, 8.9, and 13.3 kyr before present (BP) respectively, and their respective annual accumulation rates were estimated to be 27, 29, and 27 mm of ice, based upon $\delta^{18}O$ values that are considered to correlate well with annual accumulation rates [27]. The section from the 13.3 kyr BP corresponds to the beginning of the Antarctic Cold Reversal and thus is not strictly from the Holocene. Nevertheless, all three sections are more recent than the last glacial maximum and date back to or close to the Holocene. For convenience, these three sections will be referred to in this paper as "Holocene ice" even though the oldest slightly predates the Holocene. The surface snow down to a depth of 3.4 m was analyzed at a similar time-resolution to the Holocene ice [28].

Before beginning the analysis, 3 mm from the outside of each ice section was sliced off to decontaminate the surface. This was done with a clean ceramic knife on a clean bench in a cold room. The decontaminated DF sections were then cut into slices 2 mm in depth. Each slice was sealed into a clean polyethylene bag. The estimated thickness error of each sample was less than 0.5 mm. To analyze the chemical composition, an ice sample was melted and passed through a filter with 0.45 μm pores.

An ion chromatograph (Dionex 500) was used to detect the soluble ions of Cl^-, NO_3^-, SO_4^{2-}, Na^+, K^+, Mg^{2+}, and Ca^{2+}. These ions are the most important species in characterizing the chemistries of the DF ice cores. The chromatograph measured the concentrations of soluble ions with an estimated error of less than 5%. For reference, ice sections frozen from ultra-pure water were analyzed using the same method, including the same type of bag, and found no peaks on the chromatograph. This result indicates that any contamination from this method is unlikely to affect the results.

The soluble ion concentrations were also measured at 185, 362, 576, 1122, 1351, 1746, 1919, 2280, and 2413 m in depth, the same depth as the above-mentioned measurements for RS. Ice specimens of dimensions 20

× 20 × 20 mm^3 were used for analyzing ion concentrations by IC after surface decontamination using a clean ceramic knife.

The overall average ion concentrations of the DF ice sections are discussed later in this paper from the viewpoint of reconstructing the general nature of past environments in each climate period, with ion data being cited as described by Watanabe et al. [29].

3. Results and discussion

3.1. Identification of chemical compounds of water-soluble inclusions in the DF ice core by RS

The inclusions were found to typically be a few micrometers in diameter, most of them within ice grains (Fig. 2). The geometrical properties of the micro-inclusions are discussed in Section 3.3. The chemical forms of the micro-inclusions were identified from their Raman spectra. Fig. 2e–k represents the typical Raman spectra of the micro-inclusions observed. The spectra in Figs. 2e–g are identical to those for $Na_2SO_4 \cdot 10H2O$, $MgSO_4 \cdot 12H_2O$, $CaSO_4 \cdot 2H_2O$, respectively, which are hereafter referred to as simple salts. The spectra in Fig. 2h–k are not identical to any reference sample; nevertheless, it was possible to infer their compositions by examining their spectral features. SO_4^{2-} has a strong band at the symmetrical stretching mode at 955–1065 cm^{-1} and weak bands at other modes at 405–530 cm^{-1}, 580–680 cm^{-1}, 1080–1130 cm^{-1}, and 1140–1200 cm^{-1} [30]; NO_3^- has a strong band at the symmetrical stretching mode at 1015–1070 cm^{-1} and weak bands at other modes at 700–770 cm^{-1}, 800–860 cm^{-1}, and 1280–1520 cm^{-1} [22]. Spectrum *h* has features of SO_4^{2-} and NO_3^-, suggesting a compound salt containing both molecules. The spectral features of *j* and *k* are characteristic of SO_4^{2-}. The spectrum *i* nearly fits that of the MSA solution; however, the peak positions are shifted by –12 to +7 cm^{-1} and the peak widths are about one-third that of the solution. Moreover, the spectrum has sharp peaks at 2939 and 3021 cm^{-1} (not shown), which can be assigned to the C-H stretching modes of the methyl group as the MSA solution has peaks at 2942 and 3022 cm^{-1} (measured but not shown in Fig. 1). Thus, spectrum *i* is believed to be from a methane-sulfonate salt.

Several chemical species in the DF ice could not be measured with RS, such as HCl, NaCl, $MgCl_2$, $CaCl_2$, and KCl. HCl, $MgCl_2$, and $CaCl_2$ were expected to be solutions under the experimental conditions. Since these solutions only consist of monoatomic ions, they have no vibrational spectrum. Recent scanning electron microscope (SEM) observations [31] suggest that most chloride ions sit in ice lattices where they are incorporated substitutionally.

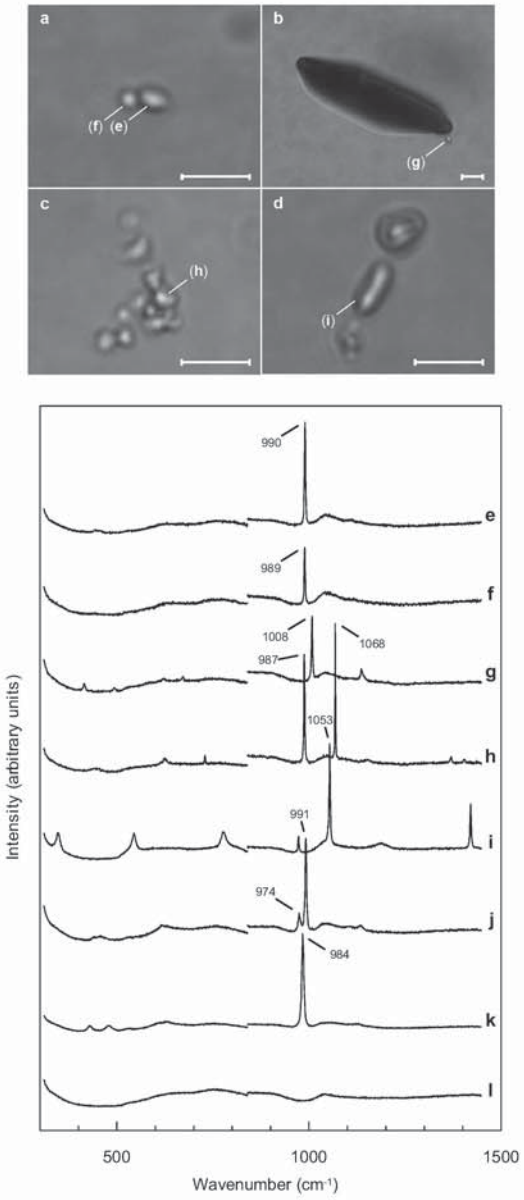

Figure 2: Micro-inclusions in the Dome Fuji ice core (left) and their Raman spectra (upper) [21]. (a) is ice from 362 m and the Holocene; (b), (c), and (d) are ice from 576 m, in the LGM. The large, black image in (b) is a plate-like inclusion; the rest of the others are micro-inclusions. The scale bar in each image is 10 μm. The Raman spectra of the labeled micro-inclusions are on the right. The spectra (e), (f), and (g) are assigned to $Na_2SO_4 \cdot 10H_2O$, $MgSO_4 \cdot 12H_2O$ and $CaSO_4 \cdot 2H_2O$, respectively. (h) is assigned to a compound salt containing SO_4^{2-} and NO_3^-. (i) is assigned to a methanesulfonate salt. (j) is assigned to a sulfate salt. The cations and combined water of the salts (h)–(k) are not confirmed. (l) is a typical spectrum of the surrounding ice showing no significant peaks in this wavenumber range. Identification of the spectra (e)–(g) was based on data obtained from prepared reference samples. The classes of the salts (h)–(k) were inferred from their spectral features.

3.2. Chemical form of micro-inclusions vs. depth (age)

The number of times a given salt appeared in 30 micro-inclusions from each of the eight depths is shown in Fig. 3. The results clearly show significant differences between the periods of cold (576 and 1919 m) and warm (the other depths).

In the Holocene ice, strong signals from $Na_2SO_4 \cdot 10H_2O$, $MgSO_4 \cdot 12H_2O$, or both were detected in all the inclusions measured. Some samples also had weak signals from $CaSO_4 \cdot 2H_2O$. In contrast, several inclusions in the LGM ice had strong peaks for $CaSO_4 \cdot 2H_2O$. Although most of the LGM spectra have not been positively identified, the following interpretations are plausible. The spectrum with the split main peak, Fig. 2j, can be interpreted as a sulfate salt. Fig. 2h shows another typical spectrum observed in the LGM ice, and can be attributed to a compound salt containing both SO_4^{2-} and NO_3^-. The spectra from several inclusions have a weak peak at 1048cm^{-1}, which may be attributed to the symmetrical stretching of NO_3^-. Insoluble inclusions identified as SiO_2 were also found in the LGM ice. The 1122 m section, which is one of the cold stages and is not shown in Fig. 3, also had strong peaks for $CaSO_4 \cdot 2H_2O$ [23] similar to the 576 and 1919 m sections. For the interstadial ice (1351 m), simple sulfate salts were the major constituents in micro-inclusions just like for the Holocene ice, but signals attributed to $CaSO_4 \cdot 2H_2O$ were stronger than for those in the Holocene ice. For the deep interglacial ice from 1746, 2280 and 2413 m, sulfate salt with a main peak at 984 cm^{-1} was a main component of micro-inclusions in addition to $Na_2SO_4 \cdot 10H_2O$, $MgSO_4 \cdot 12H_2O$, or both. This sulfonate salt is considered to be a high-pressure phase of sodium sulfonate salt [22]. A sulfonate salt with a split main peak was also observed in these three samples. The chemical form of micro-inclusions at the glacial maximum of 1919 m was similar to those of the LGM samples: $CaSO_4 \cdot 2H_2O$ dominated composition with small amount of nitrate. SiO_2 was found in some inclusions in the deep ice samples. MSA salt inclusions were observed only in the last few glacial ice cores. Sakurai et al. [32] have details about MSA sulfonates in the Dome Fuji ice.

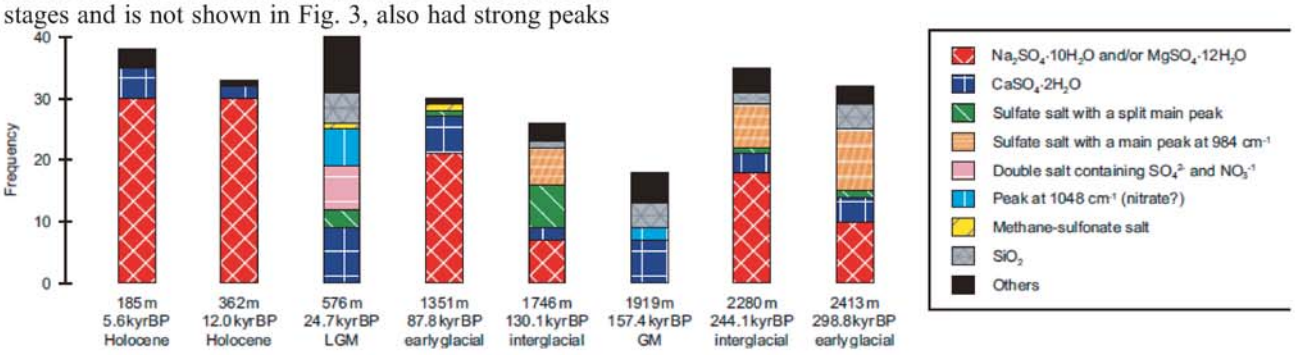

Figure 3: Observed frequencies of various salt species in 30 micro-inclusions based on micro-Raman analyses [22]. The $Na_2SO_4 \cdot 10H_2O$ and $MgSO_4 \cdot 12H_2O$ species were not distinguished because their main peaks were too close to resolve using the spectrometer. The total frequencies at a given depth did not total thirty because some inclusions contained more than one salt, or gave no signal.

Table 2: N and D are the number concentration and mean diameter of micro-inclusions, and V is the ratio of the total inclusion volume to the total ice volume [22]. For N, the values represent the mean ± standard error. For D, the numbers represent the estimated minimum and maximum values. V was estimated from N and D with consideration to the uncertainties. The margin of error for ion chromatography is less than ±0.01 μeq/l. The values in parentheses in the last four columns represent the calculated amount of ions trapped in micro-inclusions as the simple salts of $Na_2SO_4 \cdot 10H_2O$, $MgSO_4 \cdot 12H_2O$ and $CaSO_4 \cdot 2H_2O$. The 1122 m section was measured for only six ion concentrations [23].

Depth (m)	Age (kyr BP)	Temp. (°C)	N (g^{-1})	D (□m)	V	Cl^- (□eq/l)	MSA^- (□eq/l)	NO_3^- (□eq/l)	SO_4^{2-} (□eq/l)	Na^+ (□eq/l)	Mg^{2+} (□eq/l)	Ca^{2+} (□eq/l)
185	5.6 (Holocene)	−54.8	$3.5 \pm 0.4 \times 10^4$	1.7–2.5	$0.8 - 3.0 \times 10^{-7}$	2.10*	0.08*	0.46*	1.98* (0.80–3.10)	1.84* (0.67–2.54)	0.34* (0.12–0.44)	0.32* (0.02–0.10)
362	12.0 (Holocene)	−52.7	$4.0 \pm 0.5 \times 10^4$	1.8–2.7	$1.0 - 4.2 \times 10^{-7}$	2.48	0.15	0.20	1.92 (1.00–4.28)	2.15 (0.87–3.72)	0.40 (0.12–0.50)	0.52 (0.02–0.08)
576	24.7 (LGM)	−50.1	$4.3 \pm 0.4 \times 10^5$	1.4–2.3	$0.6 - 2.6 \times 10^{-6}$	5.36	0.19	1.62	4.96 (2.30–10.58)	5.29	1.78	3.10 (2.30–10.58)
1122	69.1 (early glacial)	–	–	–	–	4.40	–	1.63	4.54	4.01	1.50	2.96
1351	87.8 (early glacial)	−38.6	$1.2 \pm 0.2 \times 10^5$	1.5–2.3	$1.6 - 7.7 \times 10^{-7}$	1.08*	0.12*	0.28*	3.46* (1.56–7.76)	2.45* (1.06–5.24)	0.70* (0.18–0.92)	0.58* (0.32–1.58)
1746	130.1 (interglacial)	−31.3	$0.9 \pm 0.2 \times 10^4$	1.8–2.7	$0.2 - 1.0 \times 10^{-7}$	1.03*	0.21*	0.25*	1.98* (0.08–0.42)	1.34* (0.04–0.23)	0.58* (0.04–0.16)	0.54* (0.00–0.04)
1919	157.4 (GM)	−27.7	$7.6 \pm 0.9 \times 10^5$	1.8–2.5	$1.9 - 6.3 \times 10^{-6}$	5.25	0.28	1.89	4.64 (9.06–30.8)	4.67	2.02	3.64 (9.06–30.8)
2280	244.1 (interglacial)	−19.3	$1.4 \pm 0.3 \times 10^4$	1.8–2.6	$0.3 - 1.5 \times 10^{-7}$	0.79	0.07	0.20	1.76 (0.24–1.08)	0.45 (0.08–0.36)	0.28 (0.16–0.74)	0.40 (0.02–0.08)
2413	298.8 (early glacial)	−15.9	$1.5 \pm 0.2 \times 10^5$	1.5–2.3	$0.2 - 1.0 \times 10^{-6}$	3.08*	0.13*	0.45*	3.48* (1.68–7.62)	2.42* (0.95–4.32)	0.96* (0.54–2.46)	0.72* (0.18–0.82)

3.3. Geometrical properties and ion contents of the micro-inclusions

The geometrical properties of the micro-inclusions are shown in Table 2. The measurements show that the number concentration of micro-inclusions (*N*) is highly dependent upon the samples; for example, glacial ice contains more micro-inclusions. On the other hand, the mean size of the micro-inclusions (*D*) remained about the same independent of the samples, indicating that there was no considerable growth or dissociation of the micro-inclusions in the ice sheet. The volume fractions of micro-inclusions in a section (*Vi*) were calculated from *Ni* and *Di*.

The total amount of ions that comprised the simple salts was estimated by assuming that the micro-inclusions consisted entirely of Raman-active species [21]. This assumption was supported by an X-ray microanalysis (EDS) of micro-inclusions using a scanning electron microscope that took place at our institute. First, the total volume of the simple salts per unit volume of ice was determined as $Vi \times \langle Vs \rangle$, where *Vs* is the volume fraction of the simple salts in a given inclusion and $\langle Vs \rangle$ is the average *Vs* over all the measured inclusions. *Vs* was estimated as the integrated peak intensity of the simple salts relative to the total integrated peak intensity for a given inclusions. Second, the compositions of the simple salts were determined using the ratio of integrated Raman intensities of the main peaks in the accumulated spectra. The resulting composition ratios for $Na_2SO_4 \cdot 10H_2O$, $MgSO_4 \cdot 12H_2O$, and $CaSO_4 \cdot 2H_2O$ were 83:14:3 at 185 m, 87:11: 2 at 362 m, 0:0:100 at 576 m, 68:12:20 at 1351 m, 54:37:9 at 1746 m, 0:0:100 at 1919 m, 30:63:7 at 2280 m, and 57:32:11 at 2413 m, respectively. For these estimates, the scattering cross-section of the symmetrical stretching mode was assumed to be the same for all simple salts. A peak-fitting program (OriginLab, Origin v7) was used to distinguish overlapping peaks from $Na_2SO_4 \cdot 10H_2O$ and $MgSO_4 \cdot 12H_2O$ (Fig. 4). Lastly, the concentrations of soluble ions in the simple salts were calculated (in parentheses in Table 2) from the volume fraction and compositions of the simple salts ($Vi \times \langle Vs \rangle$) estimated above, using the molecular weights and densities of the simple salts.

To determine whether the micro-inclusions had more or less ions than the grain boundaries and veins, the estimates of ion contents in the micro-inclusions were compared to the total amount of the selected ion in the entire ice sample. The total ion concentrations were measured using conventional ion chromatography.

Although the estimated ion concentrations in the micro-inclusions include large uncertainties arising from the difficulty of measuring the size of the inclusions, it became clear that micro-inclusions are a major substance or major chemical-state for the ions included in the ice core. At least 50% of the SO_4^{2-} was from the inclusions at all four depths, and 40% or more of the Na^+ and Mg^{2+} were from the inclusions formed during warm time periods. Also, the micro-inclusions were found to generally form away from grain boundaries. Therefore, the ions that are commonly used as climate proxies appear to be preferentially bound in salts and trapped in micro-inclusions within the grains. These findings do not support previously made arguments that the climate-related signals in ice core records received serious alterations due to the diffusion of the soluble impurities through the vein system [33, 34].

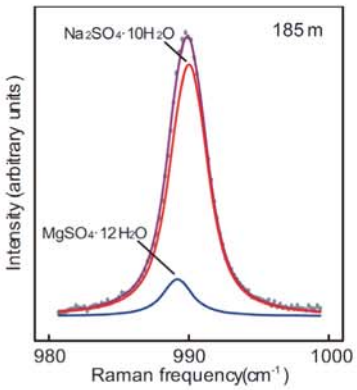

Figure 4: Peak fitting of $Na_2SO_4 \cdot 10H_2O$ and $MgSO_4 \cdot 12H_2O$ for the sum total of all spectra in the 185 m section.

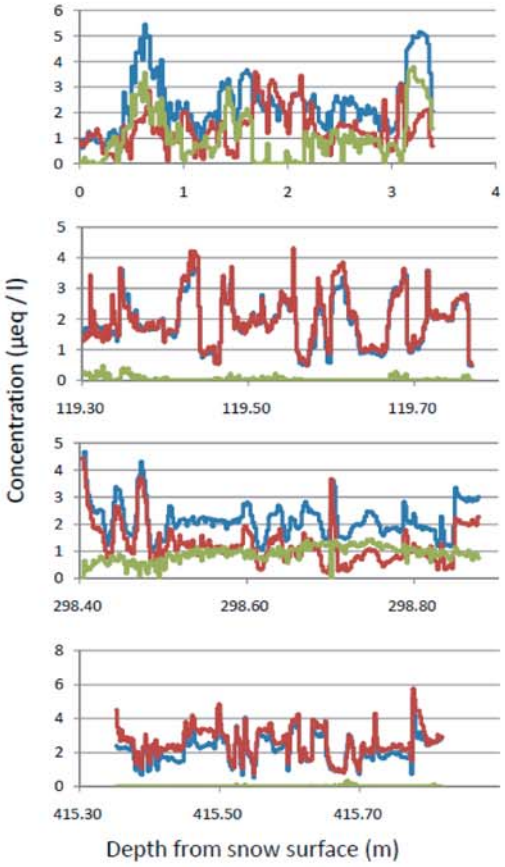

Figure 5: The depth profiles of SO_4^{2-} (blue), the sum of Na^+ and Mg^{2+} (red), and the excess SO_4^{2-} compared to sum of Na^+ and Mg^{2+} (green) with millimeter resolution during the Holocene [17].

3.4. Post-depositional $Na_2SO_4 \cdot 10H_2O$ and $MgSO_4 \cdot 12H_2O$ salt formation

The depth profiles of SO_4^{2-} and the sum of Na^+ and Mg^{2+} have fluctuation periods ranging from several millimeters to several centimeters (Fig. 5). Also, the ice sample at the depth of 298 m has slightly smoother SO_4^{2-} and sum of Na^+ and Mg^{2+} profiles than those from the 119 and 415 m depths. The profiles for the sum of Na^+ and Mg^{2+} are consistent with the recent study [35] that found that events are retained in the Na^+ and Mg^{2+} profiles. However, in contrast to that study, the SO_4^{2-} profiles examined here retained millimeter-order fluctuations in deep ice.

The surface snow had low correlation coefficients between anions and cations except for the high r^2 value (0.89) between Na^+ and Mg^{2+} (Table 3). Moreover, the ratio of Mg^{2+} to Na^+ in the surface snow is equal to that of sea salt, suggesting that is the origin for most of the Na^+ and Mg^{2+} ions. Cl^- should also be derived from the NaCl and $MgCl_2$ in sea salts; however, this is not reflected in the correlations in Table 3. The reason for the lack of correlation may be that the depth profiles of Na^+ and Cl^- in the surface snow were disturbed by various processes including 1) chemical reactions of NaCl and H_2SO_4 during transport through the atmosphere [15], 2) ion fractionation on the snow surface through sublimation and condensation [28], and 3) volatilization of HCl in the surface snow [20].

The same reasoning may apply to the depth profile of Mg^{2+}, which may have been affected by similar processes such as reactions between $MgCl_2$ and H_2SO_4. Due to these processes, the surface snow probably contains various combinations of salts (NaCl, $MgCl_2$, Na_2SO_4, and $MgSO_4$) and acids (HCl and H_2SO_4), resulting in low correlation coefficients between cations (Na^+ and Mg^{2+}) and anions (Cl^- and SO_4^{2-}).

On the other hand, the correlation coefficients between Na^+, Mg^{2+}, and SO_4^{2-} in the Holocene ice are greater than 0.9 (shaded entries in Table 3). Therefore, some redistribution process must have caused these ion pairs to become closely correlated in the deep ice. Moreover, the profile for SO_4^{2-} is nearly equal to that for the sum of Na^+ and Mg^{2+} in molar equivalents in the 119 and 415 m ice sections (Fig. 5). In the 298 m section these two profiles have the same peak and trough positions, but the amount of SO_4^{2-} generally exceeds the sum of Na^+ and Mg^{2+}. These results suggest that almost all of the Na^+ and Mg^{2+} ions in the Holocene ice co-exist with SO_4^{2-}. In the 298 m ice, 73.2% of the SO_4^{2-} is estimated to have existed in a compound with Na^+ and Mg^{2+}.

According to the thermodynamic phase diagram for Na_2SO_4 and $MgSO_4$ [36], the salts $Na_2SO_4 \cdot 10H_2O$ and $MgSO_4 \cdot 12H_2O$ should exist at the same temperature and average the same Na^+, Mg^{2+}, and SO_4^{2-} concentrations as the Holocene ice. The likelihood that these salts existed in the samples is further supported by the fact that most of the soluble impurities in the DF ice core consisted of salt inclusions within ice grains as described above and that the inclusions were primarily $Na_2SO_4 \cdot 10H_2O$ and $MgSO_4 \cdot 12H_2O$ in the Holocene ice. Taken together, these results suggest that almost all of the Na^+, Mg^{2+}, and SO_4^{2-} existed as salts in the form of $Na_2SO_4 \cdot 10H_2O$ and $MgSO_4 \cdot 12H_2O$. The formation of the post-depositional salts was mostly completed within the firn because the high correlation coefficients between Na^+, Mg^{2+}, and SO_4^{2-} occurred in the 119 m ice. These sulfate salts have a eutectic point of –1.56 and –3.67 °C for $Na_2SO_4 \cdot 10H_2O$ and $MgSO_4 \cdot 12H_2O$, respectively, and thus, would exist as a solid in both firn and ice. This solidity means that Na^+ and Mg^{2+} would have low mobility in the Holocene ice.

Table 3: Correlation coefficient matrix for the eight measured ion species in the surface snow and Holocene ice [17]. The highlighted cells are those with correlation coefficients exceeding 0.9. A: surface snow, B: 119m in depth, C: 298m in depth, and D: 415m in depth.

A	$CH_3SO_3^-$	Cl^-	NO_3^-	SO_4^{2-}	Na^+	K^+	Mg^{2+}	Ca^{2+}
$CH_3SO_3^-$	1							
Cl^-	0.05	1						
NO_3^-	0.08	−0.27	1					
SO_4^{2-}	0.30	0.26	−0.42	1				
Na^+	0.13	0.59	−0.34	0.40	1			
K^+	0.11	0.38	−0.10	0.39	0.64	1		
Mg^{2+}	0.17	0.50	−0.30	0.59	0.89	0.67	1	
Ca^{2+}	0.03	0.25	−0.27	0.25	0.21	0.11	0.25	1

B	$CH_3SO_3^-$	Cl^-	NO_3^-	SO_4^{2-}	Na^+	K^+	Mg^{2+}	Ca^{2+}
$CH_3SO_3^-$	1							
Cl^-	0.62	1						
NO_3^-	−0.02	−0.05	1					
SO_4^{2-}	−0.18	0.16	−0.15	1				
Na^+	−0.01	0.43	−0.13	0.94	1			
K^+	0.43	0.75	0.22	0.10	0.35	1		
Mg^{2+}	−0.12	0.22	−0.23	0.96	0.94	0.04	1	
Ca^{2+}	−0.02	0.34	0.41	0.22	0.33	0.45	0.20	1

C	$CH_3SO_3^-$	Cl^-	NO_3^-	SO_4^{2-}	Na^+	K^+	Mg^{2+}	Ca^{2+}
$CH_3SO_3^-$	1							
Cl^-	0.49	1						
NO_3^-	0.42	0.32	1					
SO_4^{2-}	0.13	0.36	−0.04	1				
Na^+	0.30	0.71	0.12	0.90	1			
K^+	0.24	0.70	0.23	0.49	0.69	1		
Mg^{2+}	0.33	0.57	0.11	0.93	0.95	0.62	1	
Ca^{2+}	0.28	0.53	0.25	0.36	0.53	0.62	0.48	1

D	$CH_3SO_3^-$	Cl^-	NO_3^-	SO_4^{2-}	Na^+	K^+	Mg^{2+}	Ca^{2+}
$CH_3SO_3^-$	1							
Cl^-	0.12	1						
NO_3^-	0.02	−0.19	1					
SO_4^{2-}	−0.03	0.45	−0.27	1				
Na^+	−0.04	0.54	−0.10	0.92	1			
K^+	−0.07	0.27	0.19	0.43	0.55	1		
Mg^{2+}	−0.08	0.57	−0.20	0.93	0.95	0.42	1	
Ca^{2+}	0.14	0.44	0.22	0.34	0.50	0.73	0.42	1

The excess amount of SO_4^{2-} in the 298-m section is argued here to be due to the relatively low cation concentrations in that section; this excess SO_4^{2-} exists with H^+ in the form of liquid H_2SO_4. The shape of the SO_4^{2-} profile is nearly the same as that for the sum of Na^+ and Mg^{2+}. When the two curves were subtracted, the excess SO_4^{2-} was found to have a smooth profile. The smooth profile suggests that the excess SO_4^{2-} was fully diffused as would occur in liquid H_2SO_4, which readily diffuses in firn or ice. This smoothing process of the SO_4^{2-} agrees with the finding of Barnes et al. [35].

These findings show that the salts of $Na_2SO_4 \cdot 10H_2O$ and $MgSO_4 \cdot 12H_2O$ can form within the firn when liquid-phase SO_4^{2-} diffuses around relatively immobile Na^+ and Mg^{2+}, reacts with these cations, and then becomes relatively immobile. These salts are known to also form in the atmosphere [15], and thus some salts probably originated from the firn and some from the atmosphere. Whatever the source however, the salts should be relatively immobile and have a more rapidly fluctuating profile. The key points here are that the SO_4^{2-} that forms the salts $Na_2SO_4 \cdot 10H_2O$ and $MgSO_4 \cdot 12H_2O$ becomes essentially immobile, whereas the SO_4^{2-} that forms an acid remains mobile and thus has a smooth profile.

To summarize, these findings can be explained by the following processes: 1) liquid phase SO_4^{2-} diffuses within the firn [35], 2) SO_4^{2-} becomes immobile after reacting with Na^+ or Mg^{2+}, 3) Na^+, Mg^{2+}, and SO_4^{2-} remaining as $Na_2SO_4 \cdot 10H_2O$ and $MgSO_4 \cdot 12H_2O$ salts in ice, and 4) liquid phase SO_4^{2-} remains present in the ice if the Na^+ or Mg^{2+} concentrations are insufficient to react with all of the SO_4^{2-}.

These findings also suggest that the low mobility of Na^+ and Mg^{2+} in deep ice should be useful for reconstructing the past Holocene environment with millimeter resolution, which corresponds to several months in the Holocene [27]. There will be some inherent uncertainties in the procedure; for example, the levels of $Na_2SO_4 \cdot 10H_2O$ in the ice include sources from chemical reactions in the atmosphere and thus do not solely reflect upon the past climate [15]. In addition, some years have no net snow accumulation [12]. Nevertheless, there is a need for additional climate analysis methods for the Holocene, and analyzing the levels of Na^+ and Mg^{2+} in deep ice shows promise as one.

3.5. A model for the process of water-soluble salt formation based on anion and cation priorities

As described in Section 3.4, the most important chemical compounds in salt inclusions can be identified by examining the correlation coefficients between ion species in high time-resolution profiles. This approach works well in the DF Holocene ice sections, but only reveals those compounds with a strong presence (e.g. Na_2SO_4 and $MgSO_4$ in the DF Holocene ice). Trace salts with a low ion chromatography signal cannot be identified (e.g. $CaSO_4$ in the DF Holocene). The chemical formation of salt inclusions in the whole DF ice is now discussed by considering the balance of major ion species.

The following can be considered a plausible model for the salt formation priorities of anions and cations; this analysis is based on the priority sequence listed in Table 1. Among anions, sulfate is assumed to have the highest salt formation priority due to the vaporization of HNO_3 and HCl [15, 37, 38]. These acids are easily removed from the ice until the higher priority reactions (1) and (6) reach equilibrium (priorities 1 and 2 in the sequence, as shown in Table 1). These reactions then move to the right through sulfate salt formation. Furthermore, the previous section on this topic indicated that almost all of the Na^+ and Mg^{2+} (mainly from sea salt) existed in the form of sulfate salts during the Holocene. This indicates that $NaNO_3$ and $Mg(NO_3)_2$, which come from reaction (2) between sea salts and the atmosphere, can react again to produce Na_2SO_4 and $MgSO_4$ in the atmosphere or firn. Thus, reaction (3) is assumed to be one of the most important processes in polar regions when H_2SO_4 is fully present. If reactions (1), (3), and (6) occur simultaneously with transport in the atmosphere and uppermost snow layers, HNO_3 and HCl probably pass from the snow layer aerosol into the atmosphere [17, 20, 39, 40, 41, 42]. If these reactions occur in the deeper snow and ice (i.e. below a few meters) however, then HNO_3 and HCl are probably displaced to the grain boundaries in the form of a liquid acid or solid solution in the ice crystals [43, 44]. In the latter case, the contact between liquid, highly diffusive H_2SO_4 and nitrate or chloride salts may drive the reactions.

Because carbonates have a weak acid base (CO_3^{2-}), they are considered to have a lower salt formation priority than any of the strong acid bases (SO_4^{2-}, NO_3^-, and Cl^-). This tends to promote chemical reactions (4) and (5) (priority 3 in the sequence). If there is little carbonate or H_2SO_4 but HNO_3 is fully present, then chloride salts (sea salts) can react with HNO_3 to produce nitrate salts [44, 45] (priority 4 in the sequence).

The second process to consider is the priority of sulfate formation with calcium, magnesium and sodium ions. The calcium ion may be assumed to have a higher priority than the sodium and magnesium ions, due to the ease of forming the refractory salt $CaSO_4$ (priority 1 in the sequence). In clouds, for example, the common ion effect for SO_4^{2-} produces $CaSO_4$ whenever $CaSO_4$ and Na_2SO_4 ($MgSO_4$) coexist, according to the equilibrium systems below.

$Na_2SO_4\,(MgSO_4) \leftrightarrows 2Na^+\,(Mg^{2+}) + SO_4^{2-}$
(ionization degree of nearly 1)
$CaSO_4 \leftrightarrows Ca^{2+} + SO_4^{2-}$
(ionization degree of nearly 0)

Röthlisberger et al. [20] showed in the EPICA Dome C ice core that $CaSO_4$ was more likely to form than Na_2SO_4 during the LGM, in spite of the fact that the sodium ion concentration is *higher* than the calcium ion concentration in equivalents.

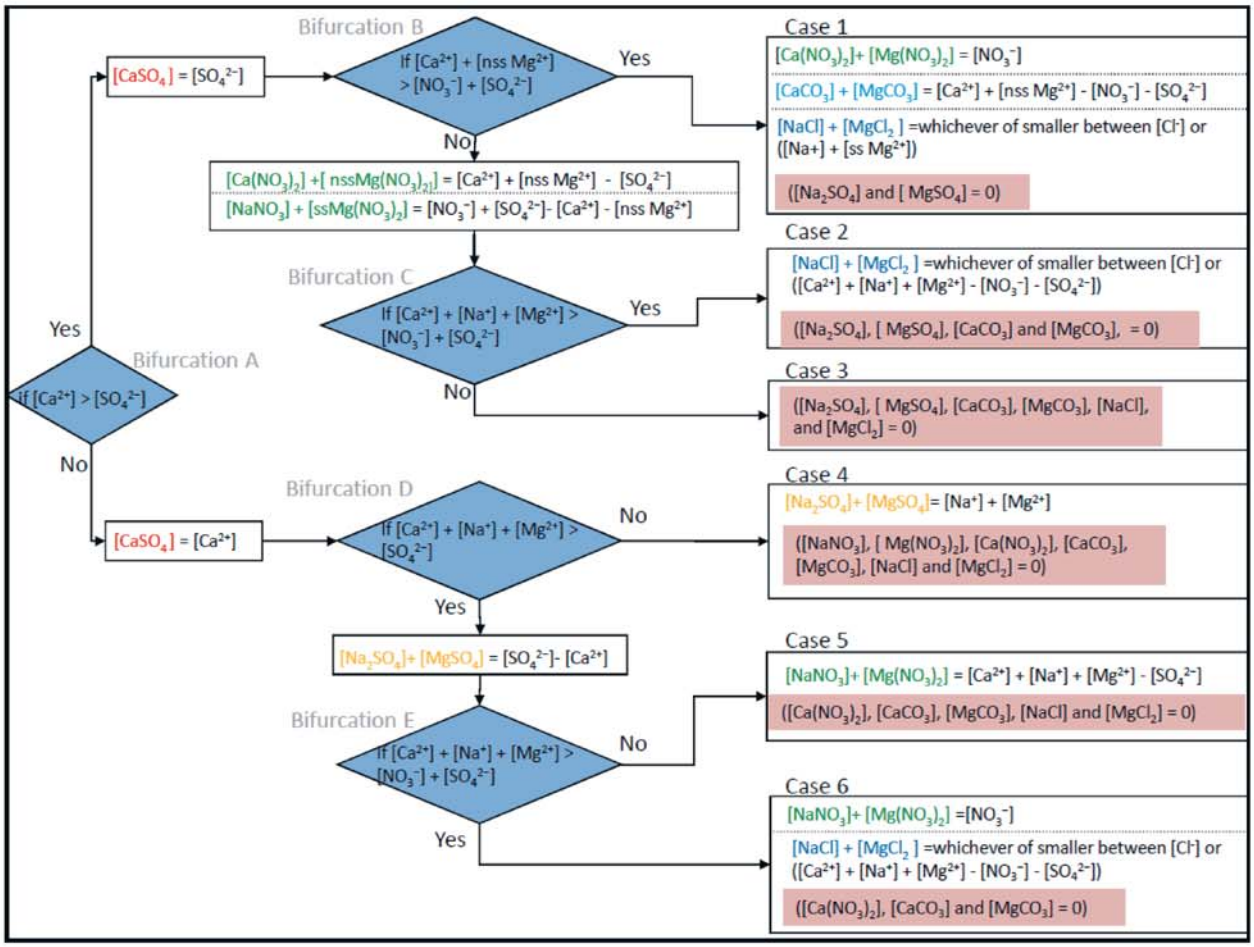

Figure 6: A bifurcation diagram charting the dominant chemical reactions between six ion species according to their relative concentrations [23]. The concentrations in equivalents of the final products can be deduced by following the appropriate bifurcations. If there are leftover anions at the terminus of the diagram (the boxes labeled case 1 to case 6), they are assumed to form acids (H_2SO_4, HNO_3, HCl).

3.6. Dominant chemical compounds of water-soluble salts as implied by the ion balance

The above arguments make it possible to deduce what kinds of salt inclusions are expected to be in the whole DF ice (Fig. 6). In this section, the contributions from sea salts (ss) to Ca^{2+} and non-sea, or terrestrial salts (nss) to Na^+ are excluded; these amounts were insignificant compared to other sources for these ions. Mg^{2+} was also subdivided into $ssMg^{2+}$ and $nssMg^{2+}$ concentrations, under the assumptions that 1) all Na^+ came from sea salt, and 2) the Mg^{2+}(μeq/l)/Na^+(μeq/l) ratio in sea salts is 0.0271 [37].

As shown in Fig. 6, $CaSO_4$ should form first, with either Ca^{2+} or SO_4^{2-} driving the reaction depending on which concentration is smaller. In the $[Ca^{2+}] > [SO_4^{2-}]$ case (Bifurcation A), excess Ca^{2+} ($[Ca^{2+}] - [SO_4^{2-}]$) and terrestrial Mg^{2+} ions form a compound with NO_3^-. If there is a cationic excess ($[Ca^{2+}] + [nssMg^{2+}] > [NO_3^-] + [SO_4^{2-}]$; Bifurcation B), then almost all the NO_3^- ions are tied up in $Ca(NO_3)_2$ and $nssMg(NO_3)_2$. The remaining Ca^{2+} and Mg^{2+} ions ($[Ca^{2+}] + [nss\ Mg^{2+}] - [NO_3^-] - [SO_4^{2-}]$) exist as $CaCO_3$ and $MgCO_3$, so almost all sea salts (NaCl and $MgCl_2$) survive. The relative concentrations of NaCl and $MgCl_2$ depend on whether ($[Na^+] + [ssMg^{2+}]$) or ($[Cl^-]$ is smaller (Case 1). If there is an anionic excess ($[Ca^{2+}] + [nss\ Mg^{2+}] < [NO_3^-] + [SO_4^{2-}]$) (Bifurcation B), then almost all the excess Ca^{2+} and terrestrial Mg^{2+} will take the form of $Ca(NO_3)_2$ and $nssMg(NO_3)_2$. In this case, the remaining NO_3^- ($[NO_3^-] + [SO_4^{2-}] - [Ca^{2+}] - [nss\ Mg^{2+}]$) exists as $NaNO_3$ and $ssMg(NO_3)_2$. If the sum of the Ca^{2+}, Na^+, and Mg^{2+} concentrations is higher than the sum of the $SO_4^{2-}$and NO_3^- concentrations in equivalent (Bifurcation C), the excess Na^+ and Mg^{2+} ($[Ca^{2+}] + [Na^+] + [Mg^{2+}] - [NO_3^-] - [SO_4^{2-}]$) exists as NaCl and $MgCl_2$. In this case the relative concentrations of NaCl and $MgCl_2$ depend on whether ($[Ca^{2+}] + [Na^+] + [Mg^{2+}] - [NO_3^-] - [SO_4^{2-}]$) or ($[Cl^-]$ is smaller (Case 2). If the sum of the Ca^{2+}, Na^+ and Mg^{2+} concentrations is less than the sum of the $SO_4^{2-}$and NO_3^- concentrations in equivalents (Bifurcation C) there are no chloride salts (Case 3).

In the case of $[Ca^{2+}] < [SO_4^{2-}]$ (Bifurcation A), excess SO_4^{2-} ($[SO_4^{2-}] - [Ca^{2+}]$) compounds with Na^+ and Mg^{2+}. If the excess SO_4^{2-} concentration is higher than the sum of the Na^+ and Mg^{2+} concentrations in equivalents (Bifurcation D), then almost all the Na^+ and Mg^{2+} ($[Mg^{2+}] + [Na^+]$) exists as Na_2SO_4 and $MgSO_4$ (Case 4)

while the leftover SO_4^{2-} exists as an acid. If the excess SO_4^{2-} concentration ($[SO_4^{2-}] - [Ca^{2+}]$) is lower than the sum of the Na^+ and Mg^{2+} concentrations (Bifurcation D), then $Mg(NO_3)_2$ and $NaNO_3$ forms instead. If the excess Ca^{2+}, Na^+ and Mg^{2+} concentration ($[Ca^{2+}] + [Na^+] + [Mg^{2+}] - [SO_4^{2-}]$) is lower than the NO_3^- concentration in equivalent (Bifurcation E), then almost all the excess Na^+ and Mg^{2+} ions form $Mg(NO_3)_2$ and $NaNO_3$ (Case 5), while any leftover NO_3^{2-} exists as an acid. If the excess Na^+ and Mg^{2+} concentrations are higher than the NO_3^- concentration in equivalent (Bifurcation E), then almost all the NO_3^- ions form $Mg(NO_3)_2$ and $NaNO_3$. In this case any leftover Na^+ and Mg^{2+} ions ($[Ca^{2+}] + [Na^+] + [Mg^{2+}] - [NO_3^-] - [SO_4^{2-}]$) exist as NaCl and $MgCl_2$ (Case 6). The proportion of NaCl to $MgCl_2$ depends on whether ($[Ca^{2+}] + [Na^+] + [Mg^{2+}] - [NO_3^-] - [SO_4^{2-}]$) or $[Cl^-]$ is smaller in equivalents.

Given the conditions and reaction branches described above, how much of each salt and acid should have existed in each section can be calculated through RS analysis (Table 4) given their measured ion concentrations. This method may be considered an improved version of the usual approach, in which one takes into account all the salt formation priorities so far discussed [10]. Note that the minor salts and three acids will always have very low estimates, as only the concentrations of the primary six ions are being taken into account. Actually, some kinds of anions (methanesulfonic ions and organic acids) and cations (ammonium ions) play an important role in more detailed interpretations [6]. The method described above, however, has the great advantage of only considering those ions which can be measured by chromatography. For reference, the ion concentrations were first analyzed using chromatography at 25 °C and 1 atm. The solubilities of the refractory salts $CaSO_4$ and $CaCO_3$ are 0.03 and 0.16 eq/l respectively. These solubilities are high enough for almost all the $CaSO_4$ and $CaCO_3$ to dissolve in the DF ice core as the sample is melted.

Table 4: Predicted concentrations of chemical compounds (μeq/l) according to the bifurcation diagram in Fig. 6 [23]. The concentrations at 119 and 298 m are calculated from the average values of the 119 and 298 m sections (Fig. 5). The lower nine depths consist of those measured by RS in Fig. 3. The orange boxes show the salt with the highest concentration in each sample.

depth (m)	age (kyr)	$CaSO_4$	Na_2SO_4+ $MgSO_4$	$Ca(NO_3)_2$+ $Mg(NO_3)_2$+ $Na(NO_3)$	NaCl+ $MgCl_2$	$MgCO_3$+ $CaCO_3$	H_2SO_4	HNO_3	HCl
Holocene	0–11	0.41	1.30	0	0	0	0.50	0.53	1.38
119	3.0	0.41	1.49	0.18	0.34	0	0	0	1.56
298	8.9	0.25	1.28	0	0	0	0.64	0.41	1.30
LGM	18–25	3.09	2.13	1.88	2.12	0	0	0	3.09
185	5.6 (Holocene)	0.32	1.66	0.46	0.06	0	0	0	2.04
362	12.0 (Termination)	0.52	1.40	0.20	0.95	0	0	0	1.53
576	24.7 (LGM)	3.10	1.86	1.62	3.59	0	0	0	1.77
1122	69.1 (early glacial)	2.96	1.58	1.63	2.30	0	0	0	2.10
1351	87.8 (early glacial)	0.29	1.44	0.28	1.08	0	0	0	0.00
1746	130.1 (interglacial)	0.27	0.72	0.25	0.66	0	0	0	0.37
1919	157.4 (GM)	1.82	0.50	1.89	3.29	0	0	0	1.96
2280	244.1 (interglacial)	0.20	0.59	0	0	0	0.29	0.20	0.79
2413	298.8 (early glacial)	0.37	1.37	0.45	1.08	0	0	0	2.00

3.7. Interpretation of chemical compounds of water-soluble salts in the whole DF ice core

In the Holocene section of the DF sample, Na_2SO_4 and $MgSO_4$ (1.30 μeq/l) were expected to be the dominant salts while $CaSO_4$ (0.41 μeq/l) plays a minor role. This is expected because of the high Na^+ and SO_4^{2-} concentrations in terms of their total concentrations (Table 4), which reflects an acidic marine atmosphere. This prediction corresponds well to the results from RS, which show that Na_2SO_4 is the dominant salt in the DF Holocene (Fig. 3). Note that the chemical concentrations in the 94 and 298 m sections correspond well to both the overall Holocene data (Table 4) and the Raman results (Fig. 3).

In the 119 m ice section, Na_2SO_4 and $MgSO_4$ (1.49 μeq/l) are the dominant salts, which still corresponds well to the overall Holocene data. However, the analysis of the ion balance implies that nitrate (0.18μeq/l) and chloride (0.34μeq/l) salts also play minor roles. This can be attributed to the high sea salt ($[Na^+]$ = 1.68 μeq/l, $[Cl^-]$ = 1.90 μeq/l) and low H_2SO_4 (1.90 μeq/l) contributions compared to the other Holocene sections. The relatively high concentration of Cl^- (1.90μeq/l) could be the result of increased accumulation during this period and its resulting reduction in post-depositional losses of HCl [20]. Indeed, the upper part of the 119 m Cl^- profile (119.291 to 119.350 m, see Fig. 5) has a high amplitude; the Cl^- profile also closely follows the Na^+ profile in this region. The combination of these facts strongly implies the presence of NaCl in the 119 m ice section.

Throughout the LGM in the DF core, $CaSO_4$ (3.09 μeq/l) should be the dominant salt. The compounds Na_2SO_4 and $MgSO_4$ (2.13μeq/l) play a minor role, as do all nitrate salts (1.88 μeq/l) and chloride salts (2.12μeq/l) (Table 4). This can be deduced from the relatively high total Ca^{2+} concentration compared to the DF Holocene sections (Table 4), which reflect a more reductive atmosphere than was present during the Holocene. This prediction corresponds well with the results from RS (Fig. 3), and is consistent with the idea that dust neutralization was an important process in the LGM ice samples of EPICA Dome C [20]. The chemical compounds deduced by this method correspond well with the results of the whole LGM section (Table 4) and to the Raman results (Fig. 3). Thus, it can be concluded that throughout the LGM $CaSO_4$ was the most important salt.

The method was checked against all the RS results in Fig. 3. Ion concentrations at the same depths are shown in Table 2. According to their respective ion balances (Table 4), the interglacial sample (130.1 kyr) should have Na_2SO_4 and $MgSO_4$ as major salts, and the glacial maximum sample (157.4 kyr) should be dominated by $CaSO_4$, nitrate salts, and chloride salts. The 1122m section corresponds to one of the cold stages of the LGP, between A4 and A5, about 70 kyr BP. The ion balance indicates that $CaSO_4$ (2.96 μeq/l) should be the dominant salt while Na_2SO_4 and $MgSO_4$ (1.58 μeq/l), nitrate salts (1.63 μeq/l), and chloride salts (2.30 μeq/l)

play minor roles (Table 4). All the other samples (87.8, 244.1, and 298.8 kyr) should be dominated by Na_2SO_4, $MgSO_4$, and chloride salts. In all sections, these deductions corresponded well with the results from RS. The only exception was for chloride salts, which cannot be identified by RS.

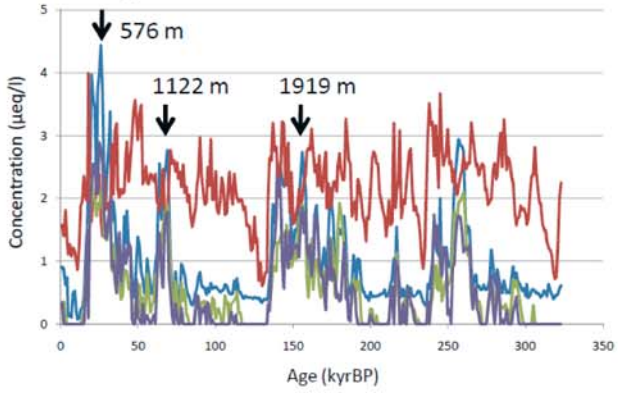

Figure 7: Predicted concentrations of chemical compounds (μeq/l) over the past 320 kyr BP in DF ice core, according to the bifurcation diagram in Fig. 6. $CaSO_4$, sum of Na_2SO_4 and $MgSO_4$, nitrate salts, and chloride salts are shown by blue, red, green, and purple, respectively. The three arrows are the depths of 576, 1122, 1919 m where $CaSO_4$ was found to be a major salt in Fig. 3 and Table 4.

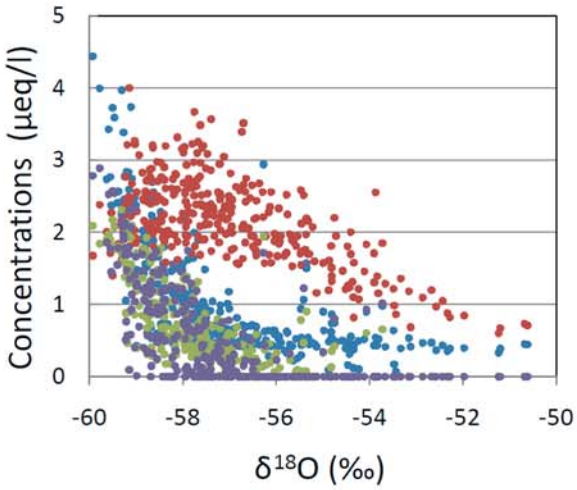

Figure 8: relationship between $\delta^{18}O$ (‰) and the concentrations of chemical compounds (μeq/l) shown in Fig.7. $CaSO_4$, sum of Na_2SO_4 and $MgSO_4$, nitrate salts, and chloride salts are shown by blue, red, green, and purple, respectively.

Finally, the soluble salts concentrations recent 340 kyr BP were reconstructed from ion data described by Watanabe et al. [29] (Figures 7 and 8). The reconstructed dominant salts were Na_2SO_4 during warm periods and $CaSO_4$ and chloride salts during cold (less than 58.5 ‰ for $\delta^{18}O$). These characteristics of the dominant salts are consistent with the interpretation of the EPICA Dome C ice core [20]. The reconstructed salts are shown to contain smaller amounts of carbonate due to the excess of strong acids (H_2SO_4, HNO_3, and HCl). The existence of lesser amounts of carbonate is consistent with the interpretation of CO_2 gas concentration in the DF ice core [10]. As described above, this method of deducing the chemical compounds in ice cores should be applicable to other polar ice cores as well. The relative concentrations of the chemical compounds mentioned in this paper are controlled mainly by atmospheric chemistry, in particular whether the polar environment is acidic or reductive and marine or continental.

4. Conclusion

This paper discussed the analysis of chemical compounds of water-soluble salts using RS and IC methods. The predictions for the dominant chemical compounds of the water-soluble salts were found to be consistent with the results from both RS and IC; namely, that sodium sulfate was mainly dominant during warm times and calcium sulfate during cold. The proposed deduction method finds the chemical compounds of the water-soluble salts using ion concentrations in ice cores. The contents of this paper contain a review of some of the authors' recent papers [17, 21, 22, 23].

Acknowledgements

The authors thank the Dome Fuji drilling team and all the participants in the JARE Dome Fuji traverse. This research was partly supported by the Ministry of Education, Science, Sports and Culture, Grants-in-Aid for Creative Scientific Research 14GS0202, Scientific Research (S) 15101001, and Young Scientists (B) 21710002. Grants-in-Aid is also thanked for the Special Education Study Expense (cooperation between universities) from MEXT and JSPS.

References

[1] Johnsen SJ, W Dansgaard, HB Clausen, CC Langway Jr. 1972. Oxygen isotope profiles through the Antarctic and Greenland ice sheets. *Nature.* 235(5339): 429–434.

[2] Petit JR, J Jouzel, D Raynaud, et al. 1999. Climate and atmospheric history of the past 420,000 years from the Vostok ice core, Antarctica. *Nature.* 399:429–436.

[3] Watanabe O, J Jouzel, S Johnsen, et al. 2003a. Homogeneous climate variability across East Antarctica over the past three glacial cycles. *Nature.* 422(6931):509–512.

[4] EPICA community members. 2006. One-to-one coupling of glacial climate variability in Greenland and Antarctica. *Nature.* 444:195–198.

[5] EPICA community members. 2004. Eight glacial cycles from an Antarctic ice core. *Nature.* 429:623–628.

[6] Legrand MR, P Mayewski. 1997. Glaciochemistry of polar ice cores: a review. *Rev. Geophys.* 35:3:219–244.

[7] Legrand MR, M de Angelis, RJ Delmas. 1984. Ion chromatographic determination of common ions at ultratrace levels in Antarctic snow and ice. *Anal. Chem. Acta*. 156:181–192.

[8] Röthlisberger R, M Bigler, MA Hutterli, et al. 2000a. Technique for continuous high-resolution analysis of trace substances in firn and ice cores. *Environ. Sci. Technol*. 34(2):338–342.

[9] Wolff EW, H Fischer, F Fundel, et al. 2006. Southern Ocean sea-ice extent, productivity and iron flux over the past eight glacial cycles. *Nature*. 440:491–496.

[10] Legrand MR, C Lorius, NI Barkov, VN Petrov. 1988. Vostok (Antarctica) ice core: atmospheric chemistry changes over the last climatic cycle (160,000 years). *Atmospheric Environment*. 22:2:317–331.

[11] Mayewski PA, LD Meeker, S Whitlow, et al. 1994. Changes in atmospheric circulation and ocean ice cover over the North Atlantic during the last 41,000 years. *Science*. 263(5154):1747–1751.

[12] Kameda T, H Motoyama, S Fujita, S Takahashi. 2008. Temporal and spatial variability of surface mass balance at Dome Fuji, East Antarctica, by the stake method from 1995 to 2006. *J. Glaciol.* 54(184):107–116

[13] Dibb JE, RW Talbot, MH Bergin. 1994. Soluble acidic species in air and snow at Summit, Greenland. *Geophys. Res. Lett*. 21(15):1627–1630.

[14] Johnsen SJ, HB Clausen, KM Cuffey, et al. 2000. Discussion of stable isotopes in polar firn and ice: the isotope effect in firn diffusion. *Physics of Ice Core Records*. ed. T Hondoh. 121–140. Sapporo: Hokkaido Univ. Press.

[15] Legrand MR, RJ Delmas. 1988. Formation of HCl in the Antarctic atmosphere. *J. Geophys. Res*. 93(D6): 7153–7168.

[16] Delmas RJ, M De Angelis, Y Fujii, et al. 2003. Linking Antarctic glaciochemical records to past climate conditions. *Mem. Natl. Inst. Polar Res., Spec. Issue*. 57:105–120.

[17] Iizuka Y, T Hondoh, Y Fujii. 2006. Na_2SO_4 and $MgSO_4$ salts during Holocene period in a Dome Fuji ice core derived by high depth-resolution analysis. *J. Glaciol.* 52:58–64.

[18] Röthlisberger R, MA Hutterli, S Sommer, et al. 2000b. Factors controlling nitrate in ice cores: evidence from the Dome C deep ice core. *J. Geophys. Res.* 105:D16:20565–20572.

[19] Kerminen VM, K Teinilä, R Hillamo. 2000. Chemistry of sea-salt particles in the summer Antarctica atmosphere. *Atmospheric Environment.* 34:2817–2825.

[20] Röthlisberger R, R Mulvaney, EW Wolff, et al. 2003. Limited dechlorination of sea salt aerosols during the last glacial period: evidence from the EPICA Dome C ice core. *J. Geophys. Res.* 108:D003604.

[21] Ohno H, M Igarashi, T Hondoh. 2005. Salt inclusions in polar ice core: location and chemical form of water-soluble impurities. *Earth Planet Sci. Lett*. 232: 171–178.

[22] Ohno, H., M. Igarashi, T. Hondoh, 2006, Characteristics of salt inclusions in polar ice from Dome Fuji, East Antarctica. *Geophys. Res. Lett. 33*, L08501.

[23] Iizuka Y, S Horikawa, T Sakurai, et al. 2008. A relationship between ion balance and the chemical compounds of salt inclusions found in the Greenland Ice Core Project and Dome Fuji ice cores. *J. Geophys. Res*. 113:D07303.

[24] Hondoh T, H Shoji, O Watanabe, et al. 2002. Depth-age and temperature prediction at Dome Fuji station, East Antarctica. *Ann. Glaciol*. 35:384– 390.

[25] Dome-F Deep Coring Group. 1998. Deep ice-core drilling at Dome Fuji and glaciological studies in east Dronning Maud Land, Antarctica. *Ann. Glaciol*. 27:333– 337.

[26] Iizuka Y, M Takata, T Hondoh, Y Fujii. 2004b. Short-term fluctuations in high special resolution profiles of soluble ions in the last glacial period of the Dome Fuji deep ice core. *Ann. Glaciol.* 39:452–456.

[27] Watanabe O, H Shoji, K Satou, et al. 2003b. Dating of the Dome Fuji, Antarctica deep ice core. *Mem. Natl Inst. Polar Res., Spec. Issue*. 57:25–37.

[28] Iizuka Y, Y Fujii, N Hirasawa, et al. 2004a. SO_4^{2-} minimum in summer snow layer at Dome Fuji, Antarctica and the probable mechanism. *J. Geophys. Res*. 109:D04307.

[29] Watanabe O, K Kamiyama, H Motoyama, et al. 2003c. General tendencies of stable isotopes and major chemical constituents of the Dome Fuji deep ice core. *Mem. Natl Inst. Polar Res., Spec. Issue*. 57:1–24.

[30] Socrates G. Table 22.1. *Infrared and Raman characteristic group frequencies: table and charts.* 3rd ed. 2001. Chichester: John Wiley & Sons Ltd., 2001.

[31] Barnes PRF, EW Wolff, DC Mallard, HM Mader. 1984. SEM studies of the morphology and chemistry of polar ice. *Microsc. Res. Tech*. 9433-9438. Reprint, 2003:62:62– 69.

[32] Sakurai, T, H Ohno, S Horikawa, et al. 2007. Data of phase diagrams and Raman spectra of H_2O-CH_3SO_3M. *The 28th Japan Symposium on*

Thermophysical Properties, Oct.24-26, Sapporo. A235:205-207.

[33] Rempel, AW, ED Waddington, JS Wettlaufer. 2001. Possible displacement of the climate signal in ancient ice by premelting and anomalous diffusion. *Nature*. 411:568–571.

[34] Rempel, AW , JS Wettlaufer, ED Waddington 2002. Anomalous diffusion of multiple impurity species: predicted implications for the ice core climate records. *J. Geophys. Res.* 107.

[35] Barnes, PRF, EW Wolff, HM Mader, et al. 2003. Evolution of chemical peak shapes in the Dome C, Antarctica, ice core. *J. Geophys. Res.* 108(D3):4126.

[36] Usdowski E, M Dietzel. 1998. Atlas and Data of Solid-Solution Equilibria of Marine Evaporites. 120–130. Berlin: Springer-Verlag.

[37] De Angelis M, JP Steffenseen, M Legrand, et al. 1997. Primary aerosol (sea salt and soil dust) deposited in Greenland ice during the last climatic cycle: comparison with east Antarctic records. *J. Geophys. Res.* 102(C12):26681–26698.

[38] Röthlisberger R, MA Hutterli, EW Wolff, et al. 2002. Nitrate in Greenland and Antarctic ice cores: a detailed description of post-depositional processes. *Ann Glacial*. 35:209–216.

[39] Bales RC, J Dibb, A Neftel. 1992. The GISP2 ice core and snow-atmosphere chemical exchange. *EOS*. 73(19):213.

[40] Dibb JE, RW Talbot, MH Bergin. 1994. Soluble acidic species in air and snow at Summit, Greenland. *Geophys. Res. Lett*. 21(15):1627–1630.

[41] Bergin MH, CI Davidson, JE Dibb, et al. 1995. Simple model to estimate atmospheric concentrations of aerosol chemical species based on snow core chemistry at Summit Greenland. *Geophys. Res. Lett*. 22(24): 3517–3520.

[42] Dibb, JE, JL Jaffrezo. 1997. Air-snow investigations at Summit Greenland. *J. Geophys. Res.* 102(D12): 26795–26807.

[43] Nye JF. 1992. Water veins and lenses in polycrystalline ice, physics and chemistry of ice. ed. N Maeno, T Hondoh. 200–205. Sapporo: Hokkaido Univ. Press.

[44] Thibert E, F Dominé. 1997. Thermodynamics and Kinetics of the Solid Solution of HCl in Ice. *J. Phys. Chem. B*. 101(18):3554 –3565.

[45] Mayewski, PA, LD Meeker, S Whitlow, et al. 1993. The atmosphere during the Younger Dryas. *Science*. 261(5118):195–197.

[46] Kerminen VM, K Teinilä, R Hillamo. 2000. Chemistry of sea-salt particles in the summer Antarctica atmosphere. *Atmospheric Environment*. 34:2817–2825.